Analyst

ROYAL SOCIETY OF CHEMISTRY

PAPER

View Article Online
View Journal

Cite this: DOI: 10.1039/d0an00268b

Quantitative analysis of direct oral anticoagulant rivaroxaban by terahertz spectroscopy†

Xu Wu,[a] Liping Wang,[a] Yan Peng, *[a,c] Fang Wu,[b] Jiumei Cao,*[b] Xiaohong Chen,[a] Wanwan Wu,[a] Huinan Yang,[a] Mengmeng Xing,[a] Yiming Zhu,*[a,c] Yijue Shi[b] and Songlin Zhuang[a,c]

Received 7th February 2020,
Accepted 20th March 2020

DOI: 10.1039/d0an00268b

rsc.li/analyst

Rivaroxaban, as a direct oral anticoagulant, has been widely used in the treatment and prevention of thrombosis disease (TD). However, even if the same dose of rivaroxaban is taken, different pathophysiological characteristics of TD patients determine the differences in plasma concentrations between individuals, leading to the difficulties of dosage selection and plasma concentration control. Conventional rivaroxaban detection methods, including prothrombin time method, anti-Xa assay and liquid chromatography-tandem mass spectrometry (LC-MS/MS), are not widely used in clinical practice due to the limitations of accuracy, speed and cost. Here, we present a simple quantitative detection method for rivaroxaban by terahertz (THz) spectroscopy. Combining density functional theory (DFT) method and THz spectroscopy, the THz absorption peaks of rivaroxaban and the corresponding low-frequency vibrational modes are studied theoretically and experimentally. We find linear relationships between the amplitudes of these characteristic peaks and the concentrations of rivaroxaban. Based on these linear functions, we can analyse the rivaroxaban concentration with a detection time of 1 minute per test and the lowest detection limit of 2 μmol mL^{-1}. As compared to Raman spectroscopy method (its detection limit is about 80 μmol mL^{-1}), our method has more potential and is practical for the clinical quantitative detection of rivaroxaban as well as other direct oral anticoagulants.

Introduction

Thrombosis disease (TD) is the leading cause of death and disability in cardiovascular diseases like myocardial infarction,[1,2] cerebrovascular diseases like cerebral infarction,[3] and lung diseases like pulmonary embolism.[4,5] In the American guidelines for antithrombotic therapy,[6,7] oral anticoagulants are recommended as the first choice for the treatment and prevention of thrombosis. Rivaroxaban is a direct oral anticoagulant, with the advantages of rapid absorption (reaches maximum plasma concentration within 2–4 hours) and high bioavailability (80%–100%).[8] It can interact directly with the blood coagulation factor Xa,[9] and then inhibit the generation of thrombin (one molecule of factor Xa can produce one thousand molecules of thrombin),[10] resulting in an enhancement in the degradability of the blood clot.[11] For these advantages, rivaroxaban has been approved by many experts including the European Society of Cardiology[12] and the American College of Chest Physicians.[13] Clinical efficacy of rivaroxaban relates closely to its concentration. However, even if TD patients take the same dose of rivaroxaban, the drug concentration varies according to the pathophysiological characteristics of different patients. These individual differences of rivaroxaban may be fatal for the patients in conditions such as before surgery, in perioperative period, with renal injury, bleeding or overdose.[14] Therefore, quick and accurate detection of rivaroxaban is important and helpful in making medical decisions, including the choice of appropriate doses and intervals, and the assessment of the risks and side effects.[15]

Conventional detection methods for rivaroxaban are mainly prothrombin time method, anti-Xa assay and liquid chromatography-tandem mass spectrometry (LC-MS/MS). Prothrombin time is the time for plasma to clot, which can reflect the concentration of rivaroxaban indirectly. However, this method has an important limitation, that is easily affected by systemic conditions such as hepatic impairment, sepsis or vitamin K deficiency.[16,17] Anti-Xa assay is another indirect detection method for rivaroxaban, whose accuracy and reliability are

[a]Terahertz Technology Innovation Research Institute, Shanghai Key Lab of Modern Optical System, Terahertz Science Cooperative Innovation Center, University of Shanghai for Science and Technology, Shanghai, P. R. China. E-mail: py@usst.edu.cn, ymzhu@usst.edu.cn
[b]Department of Geratology, Ruijin Hospital, Shanghai Jiaotong University School of Medicine, Shanghai, P. R. China. E-mail: cjm11261@rjh.com.cn
[c]Shanghai Institute of Intelligent Science and Technology, Tongji University Shanghai, P. R. China

†Electronic supplementary information (ESI) available. See DOI: 10.1039/d0an00268b

limited because its detection results are usually higher than the actual concentration of rivaroxaban.[18,19] Unlike the former two methods, LC-MS/MS can detect the concentration of rivaroxaban directly.[20,21] In LC-MS/MS detection, samples must undergo a complex pre-treatment process, to separate rivaroxaban from the sample matrix. This process brings difficulties in balancing the service life of chromatography columns and the efficiency of detection. Although many efforts have been made to solve these problems, including the use of a new sample extraction method,[22] a multi-target simultaneous detection technique,[23] and an electrospray ionization source,[24] presently LC-MS/MS is still not suitable for clinical applications as a general medical equipment. To meet the needs of clinical use, it is necessary to find a simple and economic method for the direct detection of rivaroxaban.

Terahertz (THz) spectroscopy is a promising analysis technology in the detection of biomolecules, due to its advantages of being simple, low-cost, and non-destructive and its high sensitivity to the collective motions of molecules, including the intramolecular motion, the intermolecular modes and the lattice vibrations.[25] Recently, with the assistance of specific sensors,[26–29] THz spectroscopy has achieved ultrasensitive detection of molecules and has been applied in various biomedical detections, including deoxyribonucleic acid,[30,31] metabolites,[32,33] neurotransmitters,[34,35] breathing gas,[36] and drugs.[37,38] Here we present a qualitative and quantitative detection method for rivaroxaban by THz spectroscopy and density functional theory (DFT) analysis, as well as their corresponding theoretical and experimental results. This work has a certain reference value to clinical drug monitoring in the future.

Experimental

Materials

Rivaroxaban (purity ≥ 99%, CAS: 366789-02-8), high-density polyethylene powder (HDPE, particle size: 40–48 μm, CAS: 9002-88-4), and dimethyl sulfoxide (DMSO, CAS: 67-68-5) were purchased from Sigma-Aldrich.

THz measurement

The THz spectra were obtained on a Fourier transform infrared spectrophotometer (FTIR, Bruker VERTEX 80v, signal to noise ratio ≥55 000 : 1) with 64 scans and 2 cm^{-1} spectral resolution. All THz measurements were made in the vacuum environment to reduce the impact of water vapour on the experiment.

Qualitative identification of rivaroxaban. 10 mg of rivaroxaban and 50 mg of HDPE were ground together, and compressed to form a sheet with 13 mm diameter and 0.49 ± 0.01 mm thickness. This sheet was measured by THz spectroscopy for the qualitative identification of rivaroxaban.

Quantitative detection of rivaroxaban. According to the concentration range of rivaroxaban in the human body, samples with different rivaroxaban concentrations were prepared following the steps above for the quantitative calibration. Normally, the human body does not contain any rivaroxaban itself. After rivaroxaban is ingested orally, 66% of it passes through the kidney into urine and exists in two forms: unchanged rivaroxaban (36%) and active metabolites of rivaroxaban (30%).[39] For the patients after taking 20 mg of rivaroxaban, the concentration of rivaroxaban in urine determined by anti-Xa chromogenic assays was 159.0–11 251.5 ng mL^{-1} (n = 6) (*i.e.* 0.36–25.81 μmol L^{-1}),[40] while that determined by LC-MS/MS analysis was 169 to 9579 ng mL^{-1} (n = 117) (*i.e.* 0.38–21.97 μmol L^{-1}).[41] Generally, people urinate 1.5 litres of urine every day. After general evaporation and concentration processing, 0.54–38.72 μmol of rivaroxaban can be extracted from human urine daily because it is almost insoluble in water. Then, we prepare a series of rivaroxaban/HDPE mixed sheets with a diameter of 13 mm and a weight of 200 mg (weight loss < 1%). The concentration of rivaroxaban (C_R) is calculated by eqn (1):

$$C_R = m/(M \times \pi r^2 \times d), \quad (1)$$

where m is the mass of rivaroxaban (measured by an electronic balance, precision: 0.01 mg), M is the molecular weight of rivaroxaban (435.88), d is the thickness of rivaroxaban/HDPE sheet (measured by a micrometer, precision: 0.01 mm), and r is the radius (6.5 mm) of the sheet, respectively. The C_R are 0 μmol mL^{-1}, 9.3 μmol mL^{-1}, 18.8 μmol mL^{-1}, 29.0 μmol mL^{-1}, 38.0 μmol mL^{-1}, 47.9 μmol mL^{-1}, 57.9 μmol mL^{-1}, 67.9 μmol mL^{-1}, 78.7 μmol mL^{-1}, 88.4 μmol mL^{-1} and 98.2 μmol mL^{-1}, respectively. The sheet without rivaroxaban (C_R: 0 μmol mL^{-1}) was used as the reference, and its THz spectrum was used as the reference spectrum in THz measurements.

Raman measurement

Solid rivaroxaban measurement. We prepared five 13 mm-diameter shallow pits on the glass slides, and uniformly sprinkled 1 mg, 3 mg, 5 mg, 7 mg, and 9 mg of rivaroxaban powders into these pits. These glass pits filled with different weights of rivaroxaban were used for solid Raman measurement. The Raman spectra were recorded using a laser confocal micro-Raman spectrometer (HORIBA, LabRAM HR Evolution) equipped with a laser source of 532 nm and 250 mW, 1800 gr per mm diffraction grating, and 50× working distance objective. The spectral resolution was less than 2 cm^{-1} over the spectral range of 1000–3000 cm^{-1}.

Liquid rivaroxaban measurement. We dissolved rivaroxaban powders in DMSO to prepare rivaroxaban solutions with concentrations of 0 μmol mL^{-1}, 20 μmol mL^{-1}, 40 μmol mL^{-1}, 60 μmol mL^{-1}, and 80 μmol mL^{-1}. For each rivaroxaban solution, 2 mL of the solution was filled in a quartz colorimeter cell and used for liquid Raman measurement. The Raman spectra were recorded using a self-constructed Raman spectrometer equipped with a laser source of 532 nm and 500 mW and 600 gr per mm diffraction grating. The Raman scattering light was collected using a spectrometer (HORIBA, iHR320).

Results and discussion

Qualitative identification of rivaroxaban

THz absorption peaks origin from the resonance between the THz radiation and the molecular movements that vary with different molecular structures. Therefore, we can theoretically analyse how a rivaroxaban molecule moves under the THz radiation based on its structure.

The molecular model of rivaroxaban ($C_{19}H_{18}ClN_3O_5S$, PubChem Identifier: CID 9875401)[42] that uses software Gaussian 09[43] for molecular geometry optimization and vibrational spectrum prediction is shown in Fig. 1(a). Rivaroxaban has a benzene ring and three rigid heterocyclic structures, which are an S– five-membered ring (thiophene residue), an N,O– five-membered ring and an N,O– six-membered ring, respectively. According to previous literature studies,[44–47] DFT is helpful to understand the low-frequency motion modes of molecules, especially in the case of molecules with semi-rigid groups (aromatic ring and heterocyclic structure). Therefore, we calculated the theoretical spectrum of rivaroxaban with the DFT method at the B3LYP/3-21+G level, and compared it with the experimental spectrum of rivaroxaban recorded using a FTIR spectrometer. The theoretical and experimental spectra ranging from 0.5 to 5.0 THz are shown in Fig. 1(b) and (c).

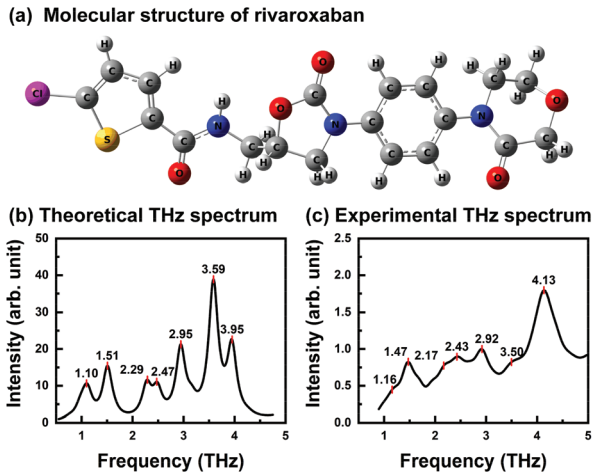

Fig. 1 (a) Molecular structure of rivaroxaban. (b) Theoretical and (c) experimental THz absorption spectra of rivaroxaban in the range of 0.5–5.0 THz.

Theoretically, rivaroxaban has seven absorption peaks, at 1.10 THz, 1.51 THz, 2.29 THz, 2.47 THz, 2.95 THz, 3.59 THz and 3.95 THz, respectively (Fig. 1(b)). Correspondingly, its experimental results (Fig. 1(c)) show four absorption peaks at 1.47 THz, 2.43 THz, 2.92 THz and 4.13 THz, as well as three shoulder peaks at 1.16 THz, 2.17 THz and 3.50 THz. These peak-positions are in good agreement with the theoretical results.

Considering the theoretical results fit well with the experimental observations, we can analyse the vibration modes of these experimental peaks based on the theoretical results. The main molecular motions of rivaroxaban are shown in Fig. 2 and Fig. S1 (ESI†). The shoulder peak at 1.16 THz, corresponding with the theoretical frequency of 1.10 THz, is associated with the out-of-plane twisting motion of the N,O– six-membered ring, together with the in-plane rocking motions of the methene and the thiophene residues [$t\omega(-NC_4H_6O_2)$ + $r(-CH_2-)$ + $r(-C_4H_2ClS)$], as shown in Fig. 2(a). The 1.47 THz peak, corresponding with the theoretical frequency of 1.51 THz, mainly originates from the out-of-plane twisting of the

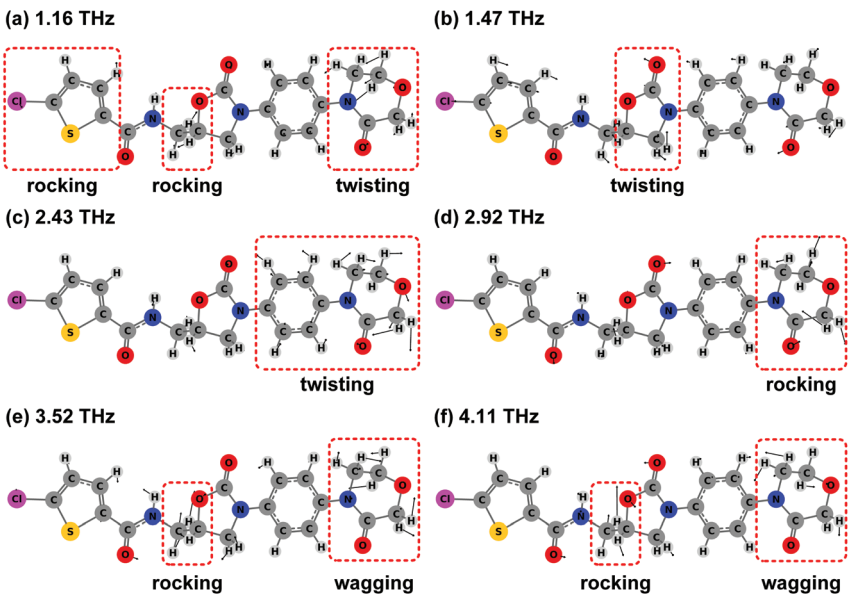

Fig. 2 Mainly molecular motions of rivaroxaban, corresponding to its THz absorption peaks in the experimental spectrum at (a) 1.16 THz, (b) 1.47 THz, (c) 2.43 THz, (d) 2.92 THz, (e) 3.52 THz and (f) 4.11 THz.

six-membered ring (tw(–$NC_4H_6O_2$), Fig. 2(b)). The shoulder peak at 2.17 THz, corresponding with the theoretical frequency of 2.29 THz, mostly originates from the out-of-plane twisting of the amide bond (tw(–CONH–), Fig. S1†). The 2.43 THz peak, corresponding with the theoretical frequency of 2.47 THz, mainly originates from the out-of-plane twisting of the benzene ring and the six-membered ring (tw(–Ph) + tw(–$NC_4H_6O_2$), Fig. 2(c)). The 2.92 THz peak, corresponding with the theoretical frequency of 2.95 THz, originates from the in-plane rocking of –COC– in the six-membered ring (r(–COC–), Fig. 2(d)). The shoulder peak at 3.52 THz, corresponding with the theoretical frequency of 3.59 THz, originates from the in-plane rocking of methane and the out-of-plane wagging of the six-membered ring (r(–CH_2) + w(–$NC_4H_6O_2$), Fig. 2(e)). The 4.11 THz peak, corresponding with the theoretical frequency of 3.95 THz, also originates from the in-plane rocking of methane and the out of plane wagging of the six-membered ring (r(–CH_2–) + w(–$NC_4H_6O_2$), Fig. 2(f)). The peaks at 3.50 THz and 4.11 THz have the same moving structure but opposite directions, which gives them different peak positions and amplitudes.

Comparisons of the THz peak positions between the experimental and theoretical results, as well as the corresponding vibrational mode assignments of the peaks, are summarized in Table 1. The main THz peaks at 1.45 THz, 2.40 THz, 2.90 THz and 4.10 THz are separated from each other and easy to identify. Therefore, these four peaks can be used as quantitative indicators of rivaroxaban identification.

Table 1 Comparison of the THz peak positions between the experimental and theoretical spectra, as well as the calculated vibrational modes of rivaroxaban

Experimental THz peak	Theoretical THz peak	Vibrational mode assignment[a]
1.16 THz shoulder peak	1.10 THz	tw(–$NC_4H_6O_2$) + r(–CH_2–) + r(–C_4H_2ClS)
1.47 THz	1.51 THz	tw(–$NC_4H_6O_2$)
2.17 THz shoulder peak	2.29 THz	tw(–CONH–)
2.43 THz	2.47 THz	tw(–Ph) + tw(–$NC_4H_6O_2$)
2.92 THz	2.91 THz	r(–COC–)
3.52 THz shoulder peak	3.63 THz	r(–CH_2–) + w(–$NC_4H_6O_2$); in the opposite directions of the motions at 4.11 THz
4.11 THz	4.01 THz	r(–CH_2–) + w(–$NC_4H_6O_2$)

[a] w, wagging; r, rocking; tw, twisting; Ph, benzene ring.

Quantitative detection of rivaroxaban

According to the concentration range of rivaroxaban in the human body, we tested samples with different rivaroxaban concentrations for the quantitative calibration. As the concentration of rivaroxaban (C_R) increased, the spectral changes in 0.5–5.0 THz, as well as the amplitude changes of the THz peaks (quantitative indicators) were observed and are shown in Fig. 3.

With C_R increasing from 0 to 98.2 μmol mL^{-1}, all the amplitudes of its THz peaks increase linearly. Here, we choose four strong peaks, at 1.45 THz, 2.40 THz, 2.90 THz and 4.10 THz, for further analysis. The corresponding functions of the regression lines are as follows: eqn (2)–(5)

$$\mathrm{Abs}_{1.45\ \mathrm{THz}} = 1.33 \times 10^{-3} \times C_R, \mathrm{SD} = 1.996, R^2 = 0.997, \quad (2)$$

$$\mathrm{Abs}_{2.40\ \mathrm{THz}} = 1.16 \times 10^{-3} \times C_R, \mathrm{SD} = 3.364, R^2 = 0.996, \quad (3)$$

$$\mathrm{Abs}_{2.90\ \mathrm{THz}} = 1.16 \times 10^{-3} \times C_R, \mathrm{SD} = 3.364, R^2 = 0.998, \quad (4)$$

$$\mathrm{Abs}_{4.10\ \mathrm{THz}} = 2.52 \times 10^{-3} \times C_R, \mathrm{SD} = 2.166, R^2 = 0.999, \quad (5)$$

where Abs is the maximum absorbance of the THz peak (arb. unit, its subscript is the corresponding peak position), C_R is the concentration of rivaroxaban (μmol mL^{-1}, calculated from eqn (1)), SD is the standard deviation of Abs (arb. unit, obtained from five repeated tests), and R^2 is the correlation coefficient of linear fitting. All R^2 in Fig. 3(b) are greater than 0.995, indicating that these four regression lines nearly perfectly fits the experimental data. These facts suggest that the THz absorption behavior of rivaroxaban agrees with the Beer–Lambert law.

The lowest detection limit (LoD) of our method is calculated according to eqn (6):

$$\mathrm{LoD} = 3 \times \mathrm{SD}_{\mathrm{lowest}}/k, \quad (6)$$

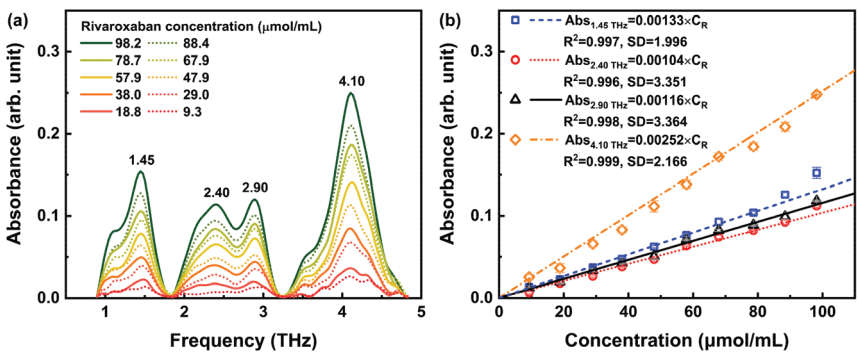

Fig. 3 (a) THz spectral changes and (b) amplitude changes of four THz peaks of rivaroxaban with an increase of its concentration. Error bars have been labeled on each data.

where SD_{lowest} is the standard deviation of Abs at the lowest detectable concentration, k is the slope of the linear fitting. Here LoD is 4.56 μmol mL^{-1} for the 1.45 THz peak, 4.36 μmol mL^{-1} for the 2.40 THz peak, 2.03 μmol mL^{-1} for the 2.90 THz peak, and 3.80 μmol mL^{-1} for the 4.10 THz peak, respectively.

Comparison with Raman spectroscopy

Similar to THz spectroscopy, Raman spectroscopy is a non-destructive analysis method. So we also used Raman spectroscopy to detect samples with different rivaroxaban concentrations, in both solid and liquid sample states. The results are shown in Fig. 4.

Fig. 4(a) and (b) show the Raman spectral changes and the corresponding Raman intensity changes of rivaroxaban with its mass increasing from 1 mg to 9 mg. In the Raman shift range of 1300–1700 cm^{-1}, three strong peaks at 1428 cm^{-1}, 1463 cm^{-1}, and 1526 cm^{-1}, as well as two small peaks at 1604 cm^{-1} and 1639 cm^{-1} are observed. These peaks are consistent with the Raman spectra recorded by Grunenberg *et al.*,[48] indicating that they are Raman characteristic peaks of rivaroxaban. However, the intensities of these peaks do not

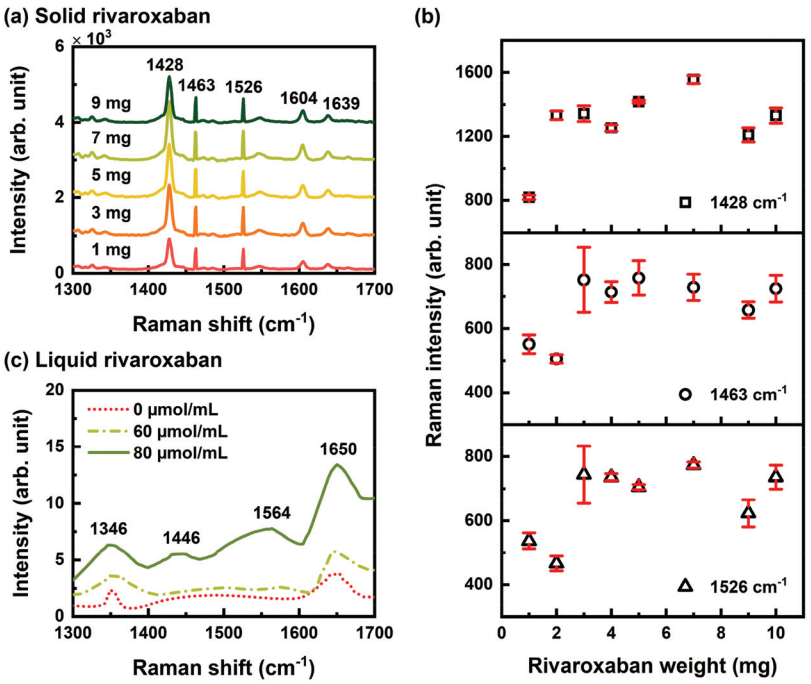

Fig. 4 Raman spectra of rivaroxaban with different sample states: (a) solid rivaroxaban and (c) liquid rivaroxaban. (b) Raman intensity changes of rivaroxaban with its mass increasing from 1 mg to 9 mg. Error bars have been labeled on each data.

Table 2 The lowest detection limit, the advantages and disadvantages of the conventional methods, the Raman spectroscopy method, and our method in the quantitative detection of rivaroxaban

Method	LoD[a]	Advantages	Disadvantages
PT/INR method[a 17]	Non-quantitative	Widely available	(a) Poor sensitivity (b) Easily affected by systemic conditions of patients
Anti-factor Xa assay[17]	≥30 μg L^{-1}	Highly sensitive	(a) Need specific calibrators (b) Not yet available in every laboratory (c) High cost
LC-MS/MS[20–24]	2–3 μg L^{-1}	Monitoring of multiple reactions	(a) Need isotope-labeled standard solution (b) Need complicated chemical treatment (c) High cost
Raman spectroscopy (this work)	~80 μmol mL^{-1}	(a) Physical method (b) Molecular recognition with multiple Raman peaks	(a) Limited detection range (b) Laser-induced sample damage
THz spectroscopy (this work)	2 μmol mL^{-1}	(a) Physical method (b) Molecular recognition with multiple THz peaks (c) Without complicated chemical treatment	Its LoD should be further reduced

[a] LoD: lowest detection limit; PT: prothrombin time; INR: international normalized ratio.

increase with the mass of rivaroxaban (Fig. 4(b)). This result diverges from the Beer–Lambert law. This is because the detection range of Raman spectrometer is only 0.5–1 μm in the radius and 1–2 μm in the depth, which is limited by the laser wavelength and the objective lens used in this instrument.

Fig. 4(c) shows the Raman spectral changes of rivaroxaban/DMSO solutions with the rivaroxaban concentration increasing from 0 μmol mL^{-1} to 80 μmol mL^{-1}. In the Raman shift range of 1300–1700 cm^{-1}, the peaks at 1346 cm^{-1} and 1650 cm^{-1} originate from the solvent DMSO, while the peaks at 1446 cm^{-1} and 1564 cm^{-1} originate from rivaroxaban. Until the rivaroxaban concentration increases to 80 μmol mL^{-1}, its Raman characteristic peaks can be observed. This fact indicates that the detection limit of the Raman spectroscopy method is more than 80 μmol mL^{-1}. While the lowest detection limit of our method is as low as 2.03 μmol mL^{-1}. Therefore, our method has more potential than the Raman spectroscopy method in the detection of rivaroxaban.

Table 2 shows the comparison of the characteristics of the conventional methods, the Raman spectroscopy method, and our method in the quantitate detection of rivaroxaban. Compared with other methods, our method has advantages of direct recognition of rivaroxaban molecules, of being a quantitative model based on many indexes (THz absorption peaks of rivaroxaban), and of not involving a complicated chemical treatment. We will further reduce the LoD of our method through different approaches of THz signal improvement.[49] Considering these characteristics, our method can be used as a complementary method to monitor rivaroxaban in the future.

Conclusions

Here we present a low-cost, accurate (four quantitative indicators) detection method for direct oral anticoagulant rivaroxaban, by DFT method and THz spectroscopy. Based on the DFT method, we theoretically investigated the THz absorption peaks and the corresponding vibration modes of rivaroxaban. By using a FTIR spectrometer, we recorded the experimental THz spectrum of rivaroxaban in the range of 0.5–5.0 THz. It was in good agreement with the theoretical spectrum. With these results, we made it clear that the THz peaks at 1.45 THz, 2.40 THz, 2.90 THz and 4.10 THz are four important indicators in the rivaroxaban identification. Then we carried out a series of tests for different rivaroxaban concentrations. The amplitudes of these four characteristic peaks all linearly increased with the concentration of rivaroxaban from 0 to 98.2 μmol mL^{-1}. This range covers the rivaroxaban concentrations in the human urine. For the patients taking 20 mg of rivaroxaban every day, 0.54–38.72 μmol of rivaroxaban will be found in the urine. Therefore, rivaroxaban can be detected by the linear functions of its THz peak amplitudes and non-intrusive urine sampling. Also, we compared this method with Raman spectroscopy, and found that the lowest detection limit of Raman spectroscopy method is much higher than our method. Based on the above results, our method shows the properties of being simple, economic, and non-destructive, as well as provides the advantages of recognition at the molecular level and multi-quantitative indicators. This method may be helpful for the clinical monitoring of rivaroxaban and other related drugs in the future.

Conflicts of interest

There are no conflicts to declare.

Acknowledgements

The authors would like to thank the National Major Project of Scientific Instrument and Equipment Development (2017YFF0106300); the National Natural Science Foundation of China (61805140, 61922059, 61771314 and 81961138014); the 111 Project (D18014); the International Joint Lab Program supported by the Shanghai Science and Technology Committee (17590750300); and the Key Project supported by the Shanghai Science and Technology Committee (YDZX20193100004960) for funding.

References

1 A. B. Chandler, I. Chapman, L. R. Erhardt, W. C. Roberts, C. J. Schwartz, D. Sinapius, D. M. Spain, S. Sherry, P. M. Ness and T. L. Simon, *Am. J. Cardiol.*, 1974, **34**, 823–833.
2 G. Lippi, M. Franchini and G. Targher, *Nat. Rev. Cardiol.*, 2011, **8**, 502–512.
3 J. Stam, *N. Engl. J. Med.*, 2005, **352**, 1791–1798.
4 M. D. Silverstein, J. A. Heit, D. N. Mohr, T. M. Petterson, W. M. O'Fallon and L. J. Melton III, *Arch. Intern. Med.*, 1998, **158**, 585–593.
5 J. A. Heit, M. D. Silverstein, D. N. Mohr, T. M. Petterson, W. M. O'Fallon and L. J. Melton III, *Arch. Intern. Med.*, 2000, **160**, 809–815.
6 A. Holbrook, S. Schulman, D. M. Witt, P. O. Vandvik, J. Fish, M. J. Kovacs, P. J. Svensson, D. L. Veenstra, M. Crowther and G. H. Guyatt, *Chest*, 2012, **141**, e152S–e184S.
7 W. Ageno, A. S. Gallus, A. Wittkowsky, M. Crowther, E. M. Hylek and G. Palareti, *Chest*, 2012, **141**, e44S–e88S.
8 D. Kubitza, M. Becka, B. Voith, M. Zuehlsdorf and G. Wensing, *Clin. Pharmacol. Ther.*, 2005, **78**, 412–421.
9 E. Perzborn, J. Strassburger, A. Wilmen, J. Pohlmann, S. Roehrig, K. H. Schlemmer and A. Straub, *J. Thromb. Haemostasis*, 2005, **3**, 514–521.
10 J. Ansell, *J. Thromb. Haemostasis*, 2007, **5**, 60–64.
11 R. Varin, S. Mirshahi, P. Mirshahi, J. Chidiac, G. Kierzek, J.-P. Marie, M. Mirshahi, C. Soria and S. Jeannette, *Blood*, 2009, **114**, 1064–1064.
12 P. Kirchhof, S. Benussi, D. Kotecha, A. Ahlsson, D. Atar, B. Casadei, M. Castella, H.-C. Diener, H. Heidbuchel, J. Hendriks, G. Hindricks, A. S. Manolis, J. Oldgren,

B. A. Popescu, U. Schotten, B. Van Putte, P. Vardas and E. S. C. S. D. Group, *Eur. Heart J.*, 2016, **37**, 2893–2962.

13 J. J. You, D. E. Singer, P. A. Howard, D. A. Lane, M. H. Eckman, M. C. Fang, E. M. Hylek, S. Schulman, A. S. Go, M. Hughes, F. A. Spencer, W. J. Manning, J. L. Halperin and G. Y. H. Lip, *Chest*, 2012, **141**, e531S–e575S.

14 W. Mueck, A. W. A. Lensing, G. Agnelli, H. Décousus, P. Prandoni and F. Misselwitz, *Clin. Pharmacokinet.*, 2011, **50**, 675–686.

15 W. Mueck, J. Stampfuss, D. Kubitza and M. Becka, *Clin. Pharmacokinet.*, 2014, **53**, 1–16.

16 Y. C. Barrett, Z. Wang, C. Frost and A. Shenker, *Thromb. Haemostasis*, 2010, **104**, 1263–1271.

17 E. Lindhoff-Last, J. Ansell, T. Spiro and M. M. Samama, *Ann. Med.*, 2013, **45**, 423–429.

18 J. Douxfils, A. Tamigniau, B. Chatelain, C. Chatelain, P. Wallemacq, F. Mullier and J.-M. Dogné, *Thromb. Haemostasis*, 2013, **110**, 723–731.

19 O. Königsbrügge, P. Quehenberger, S. Belik, G. Weigel, C. Seger, A. Griesmacher, I. Pabinger and C. Ay, *Ann. Hematol.*, 2015, **94**, 1463–1471.

20 G. Rohde, *J. Chromatogr. B: Anal. Technol. Biomed. Life Sci.*, 2008, **872**, 43–50.

21 E. M. H. Schmitz, K. Boonen, D. J. A. Van Den Heuvel, J. L. J. Van Dongen, M. W. M. Schellings, J. M. A. Emmen, F. Van Der Graaf, L. Brunsveld and D. Van De Kerkhof, *J. Thromb. Haemostasis*, 2014, **12**, 1636–1646.

22 J. Kuhn, T. Gripp, T. Flieder, A. Hammerschmidt, D. Hendig, I. Faust, C. Knabbe and I. Birschmann, *Clin. Chim. Acta*, 2018, **486**, 347–356.

23 K. Foerster, A. Huppertz, A. Meid, O. Müller, T. Rizos, L. Tilemann, W. Haefeli and J. Burhenne, *Anal. Chem.*, 2018, **90**, 9395–9402.

24 J. Lagoutte-Renosi, J. Le Poupon, A. Girard, D. Montange and S. Davani, *J. Chromatogr. B: Anal. Technol. Biomed. Life Sci.*, 2018, **1100**, 43–49.

25 D. Plusquellic, K. Siegrist, E. Heilweil and O. Esenturk, *ChemPhysChem*, 2007, **8**, 2412–2431.

26 J. Kitagawa, T. Ohkubo, M. Onuma and Y. Kadoya, *Appl. Phys. Lett.*, 2006, **89**, 041114.

27 P. Tang, J. Li, L. Du, Q. Liu, Q. Peng, J. Zhao, B. Zhu, Z. Li and L. Zhu, *Opt. Express*, 2018, **26**, 30655–30666.

28 M. S. Islam, J. Sultana, K. Ahmed, M. R. Islam, A. Dinovitser, B. W.-H. Ng and D. Abbott, *IEEE Sens. J.*, 2018, **18**, 575–582.

29 B. K. Paul, K. Ahmed, D. Vigneswaran, F. Ahmed, S. Roy and D. Abbott, *IEEE Sens. J.*, 2018, **18**, 9948–9954.

30 M. Nagel, F. Richter, P. Haring-Bolívar and H. Kurz, *Phys. Med. Biol.*, 2003, **48**, 3625–3636.

31 A. Arora, T. Q. Luong, M. Krüger, Y. J. Kim, C.-H. Nam, A. Manz and M. Havenith, *Analyst*, 2012, **137**, 575–579.

32 P. C. Upadhya, Y. C. Shen, A. G. Davies and E. H. Linfield, *J. Biolo. Phys.*, 2003, **29**, 117–121.

33 X. Wu, Y. Dai, L. Wang, Y. Peng, L. Lu, Y. Zhu, Y. Shi and S. Zhuang, *Biomed. Opt. Express*, 2020, **11**, 963–970.

34 Z. Zhu, C. Cheng, C. Chang, G. Ren, J. Zhang, Y. Peng, J. Han and H. Zhao, *Analyst*, 2019, **144**, 2504–2510.

35 Y. Peng, X. Yuan, X. Zou, W. Chen, H. Huang, H. Zhao, B. Song, L. Chen and Y. Zhu, *Biomed. Opt. Express*, 2016, **7**, 4472–4479.

36 N. Rothbart, O. Holz, R. Koczulla, K. Schmalz and H.-W. Hübers, *Sensors*, 2019, **19**, 2719.

37 A. D. Burnett, W. Fan, P. C. Upadhya, J. E. Cunningham, M. D. Hargreaves, T. Munshi, H. G. M. Edwards, E. H. Linfield and A. G. Davies, *Analyst*, 2009, **134**, 1658–1668.

38 K. Ajito, *IEEE Trans. Terahertz Sci. Technol.*, 2015, **5**, 1140–1145.

39 C. Weinz, T. Schwarz, D. Kubitza, W. Mueck and D. Lang, *Drug Metab. Dispos.*, 2009, **37**, 1056.

40 J. Harenberg, S. Du, M. Wehling, S. Zolfaghari, C. Weiss, R. Krämer and J. Walenga, *Clin. Chem. Lab. Med.*, 2016, **54**, 275–283.

41 J. Harenberg, U. Warttinger, S. Hetjens, R. Schreiner, C. Giese, H. J. Roth and C. Weiss, in International Society on Thrombosis and Haemostasis (ISTH) 2017 Congress, Berlin, July 08-13, 2017.

42 PubChem Identifier: CID 9875401 URL: https://pubchem.ncbi.nlm.nih.gov/compound/9875401#section=3D-Conformer.

43 M. J. Frisch, G. W. Trucks, H. B. Schlegel, G. E. Scuseria, M. A. Robb, J. R. Cheeseman, G. Scalmani, V. Barone, B. Mennucci, G. A. Petersson, H. Nakatsuji, M. Caricato, X. Li, H. P. Hratchian, A. F. Izmaylov, J. Bloino, G. Zheng, J. L. Sonnenberg, M. Hada, M. Ehara, K. Toyota, R. Fukuda, J. Hasegawa, M. Ishida, T. Nakajima, Y. Honda, O. Kitao, H. Nakai, T. Vreven, J. A. Montgomery Jr., J. E. Peralta, F. Ogliaro, M. Bearpark, J. J. Heyd, E. Brothers, K. N. Kudin, V. N. Staroverov, R. Kobayashi, J. Normand, K. Raghavachari, A. Rendell, J. C. Burant, S. S. Iyengar, J. Tomasi, M. Cossi, N. Rega, J. M. Millam, M. Klene, J. E. Knox, J. B. Cross, V. Bakken, C. Adamo, J. Jaramillo, R. Gomperts, R. E. Stratmann, O. Yazyev, A. J. Austin, R. Cammi, C. Pomelli, J. W. Ochterski, R. L. Martin, K. Morokuma, V. G. Zakrzewski, G. A. Voth, P. Salvador, J. J. Dannenberg, S. Dapprich, A. D. Daniels, O. Farkas, J. B. Foresman, J. V. Ortiz, J. Cioslowski and D. J. Fox, *Gaussian 09 Revision A.01*, Gaussian, Inc., Wallingford CT, 2009.

44 P. M. Hakey, D. G. Allis, W. Ouellette and T. M. Korter, *J. Phys. Chem. A*, 2009, **113**, 5119–5127.

45 Q. Song, Y. Zhao, R. Zhang, X. Liu, L. Dong and W. Xu, *J. Infrared, Millimeter, Terahertz Waves*, 2010, **31**, 310–318.

46 W. Chen, Y. Peng, X. Jiang, J. Zhao, H. Zhao and Y. Zhu, *Sci. Rep.*, 2017, **7**, 12166.

47 T. Li, H. Ma, Y. Peng, X. Chen, Z. Zhu, X. Wu, T. Kou, B. Song, S. Guo, L. Liu and Y. Zhu, *Biomed. Opt. Express*, 2018, **9**, 5467–5476.

48 A. Grunenberg, J. Lenz, G. A. Braun, B. Keil and C. R. Thomas, *U.S. Patent*,8188270, 2012.

49 Y. Peng, C. Shi, Y. Zhu, M. Gu and S. Zhuang, *PhotoniX*, 2020, **1**, 12.